Science AAAS

Strain Tuning of Individual Atomic Tunneling Systems Detected by a Superconducting Qubit

Grigorij J. Grabovskij *et al.*

Science **338**, 232 (2012);
DOI: 10.1126/science.1226487

Strain Tuning of Individual Atomic Tunneling Systems Detected by a Superconducting Qubit

Grigorij J. Grabovskij, Torben Peichl, Jürgen Lisenfeld, Georg Weiss,* Alexey V. Ustinov*

In structurally disordered solids, some atoms or small groups of atoms are able to quantum mechanically tunnel between two nearly equivalent sites. These atomic tunneling systems have been identified as the cause of various low-temperature anomalies of bulk glasses and as a source of decoherence of superconducting qubits where they are sparsely present in the disordered oxide barrier of Josephson junctions. We demonstrated experimentally that minute deformation of the oxide barrier changes the energies of the atomic tunneling systems, and we measured these changes by microwave spectroscopy of the superconducting qubit through coherent interactions between these two quantum systems. By measuring the dependence of the energy splitting of atomic tunneling states on external strain, we verify a central hypothesis of the two-level tunneling model for disordered solids.

At low temperatures (below 1 K), specific heat and thermal conductivity of amorphous solids deviate markedly from predictions based on long-wavelength phonons in a three-dimensional elastic solid (*1*). To explain this behavior, which is independent of chemical composition, it has been suggested by Phillips (*2*) and Anderson *et al*. (*3*) that in the irregular structure of a disordered solid, some atoms or small groups of atoms experience a potential landscape that allows them to occupy two almost-equivalent sites. This situation is modeled by two potential wells of similar depth separated by an energy barrier (Fig. 1). For plausible parameter values, the tunneling of the atomic entity gives rise to low-energy excitations that are effective in the temperature range below 1 K. Disregarding higher-level vibrational excitations, this is equivalent to a two-level tunneling system (TLS) with an energy splitting $E = \sqrt{\Delta_0^2 + \Delta^2}$, where Δ_0 is the tunneling energy related to the overlap of the wave functions of the particle in either of the two wells, and Δ is the energy difference between the two minima of the double-well potential (Fig. 1). In an amorphous solid, the values of both Δ_0 and Δ have broad distributions. Phenomenologically, the low-temperature thermal anomalies mentioned above and further dynamical properties can be accounted for if an essentially constant density of TLS states $n(E)$ is assumed (*4*–*6*).

Atomic TLSs are believed to be a source of noise and decoherence for various solid-state circuits (*7*–*10*), as well as nanomechanical (*11*, *12*) and optomechanical devices (*13*); ensembles of TLSs are thought to be the major general source of decoherence for superconducting qubits and microwave resonators. In particular, the quantum coherence times of qubits based on Josephson junctions (JJs) were found to be largely affected by the presence of TLSs located predominantly in the tunnel barriers of the junctions (*7*, *8*), which are typically made of a 2- to 3-nm-thick layer of disordered aluminum oxide. Spectroscopic measurements indicate individual coherent TLSs resonantly interacting with the qubits (*7*, *14*–*16*). Some TLSs exhibited coherence times much longer than those of the superconducting qubits (*16*–*18*) and, hence, can themselves be used as effective quantum memories (*19*) or computational qubits for testing quantum information protocols (*20*, *21*).

However, these experiments with TLSs are limited by the fact that TLS properties can not be predicted or controlled at will (*7*, *14*–*21*). An individual JJ qubit has its own random distribution of TLS frequencies. Individual coherent TLSs remain rather stable at temperatures below 1 K, but thermal cycling to room temperature completely changes TLS frequencies and their coupling strength to the qubit. These unpredictable properties represent a major obstacle to potential usage of coherent TLSs in hybrid quantum circuits.

Here, we report an experiment in which we tune the energy of coherent TLSs coupled resonantly to a JJ qubit. When varying a static strain field in situ and performing microwave spectroscopy of the junction, we observe continuously changing energies of individual coherent TLSs.

Information on how TLSs couple to strain fields comes mainly from ultrasonic measurements on glasses (*4*–*6*). However, these measurements only reveal the mean response of a huge number of TLSs, averaging over their individual coupling strengths and essentially ignoring the tensorial character of the strain field. General arguments (*4*, *22*) suggest that coupling to strain fields occurs mainly through a change of the asymmetry Δ of the double-well potential (Fig. 1), whereas changes of Δ_0 are negligible. The Hamiltonian of a TLS in the localized representation may thus be written as

$$H = \frac{1}{2}\begin{pmatrix} \Delta & -\Delta_0 \\ -\Delta_0 & -\Delta \end{pmatrix} + \frac{1}{2}\begin{pmatrix} \delta\Delta & 0 \\ 0 & -\delta\Delta \end{pmatrix} \quad (1)$$

with $\delta\Delta = 2\gamma\varepsilon$, where $\gamma = 1/2\partial\Delta/\partial\varepsilon$ describes the variation of the asymmetry with the (dimensionless) strain field ε (*23*). For static strain, the two terms of the Hamiltonian may be added (that is, the strain-induced $\delta\Delta$ adds to the intrinsic asymmetry Δ) to give, in the representation of the then-valid eigenstates, an energy splitting (*23*)

$$E = \sqrt{\Delta_0^2 + (\Delta + \delta\Delta)^2} \quad (2)$$

To verify this $E(\varepsilon)$ dependence, we tuned the TLS asymmetry energy $\Delta + \delta\Delta$ by bending the sample while tracking the TLS energy E with a resonantly coupled JJ qubit.

To detect individual TLSs, we used a Josephson tunnel junction operated as a phase qubit (*24*). The measurement circuit (Fig. 2) consists of a superconducting loop interrupted by a JJ. The phase qubit forms an *LC*-resonator, where L comprises the loop inductance and the nonlinear inductance of the JJ, and C is the junction capacitance. Quantum dynamics of the qubit is determined by the charge on the capacitor and the phase drop across the junction acting as conjugated variables. Because the charge is subject to large quantum uncertainties caused by the relatively large capacitance, the qubit states $|0\rangle$ and $|1\rangle$ are the two phase eigenstates of lowest energy in a metastable potential well. The energy difference of these two states can be tuned by applying an external flux bias Φ_{ext} to the qubit.

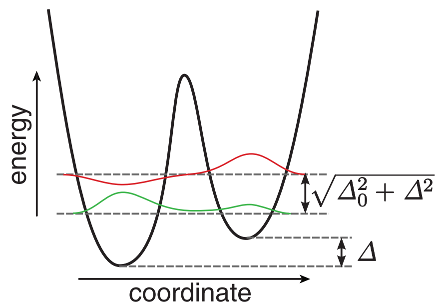

Fig. 1. Sketch of a double-well potential. The figure shows the two eigenstates with energy splitting $E = \sqrt{\Delta_0^2 + \Delta^2}$ and respective wave functions, built from the two localized states as symmetric and antisymmetric combinations. The tunneling energy Δ_0 depends on microscopic details and may be written as $\Delta_0 = \hbar\Omega\exp(-\lambda)$, where Ω is a typical vibrational frequency, $\lambda = d\sqrt{2mV_0}/\hbar$, m is the mass of the tunneling particle, d is the distance between the two potential wells along the appropriate configuration coordinate, $V_0 >> \hbar\Omega$ is the potential barrier, and $\hbar$ is Planck's constant divided by 2π.

Physikalisches Institut and Deutsche Forschungsgemeinschaft (DFG) Center for Functional Nanostructures (CFN), Karlsruhe Institute of Technology, 76128 Karlsruhe, Germany.

*To whom correspondence should be addressed. E-mail: alexey.ustinov@kit.edu (A.V.U.); georg.weiss@kit.edu (G.W.)

In a qubit spectrum (Fig. 3A), for each value of Φ_{ext}, microwave pulses of varying frequency are applied to the qubit, which initially has been prepared in its ground state. The pulses are sufficiently long to generate an equal population probability of the two qubit states if the microwave frequency is at resonance, whereas off-resonance microwave pulses leave the qubit in its ground state. To read out the qubit, a bias flux pulse of 1-ns duration is applied to lower the potential barrier of the metastable well such that only the excited qubit state has a high probability of escaping from the well. This escape is associated with a change of the flux in the qubit loop, which is finally detected by an inductively coupled superconducting quantum interference device (SQUID) operated as a magnetometer. The spectrum thus reflects the probability $P(|1\rangle)$ of the qubit to be in state $|1\rangle$ after applying the microwave pulse.

The spectrum of the JJ qubit (Fig. 3A) clearly shows avoided level crossings, which have been attributed to the qubit's coherent interaction with individual TLSs (*7*, *14*–*16*). The coupling strength v equals the frequency gap in the avoided level crossing (Fig. 3A, inset), and the center of the anticrossing corresponds to the TLS energy $E = hf_{TLS}$, where h is Planck's constant and f_{TLS} is the TLS resonance frequency. Although alternative theoretical models of two-level systems have been proposed to explain the avoided level crossings observed in qubit spectroscopy data (*25*–*28*), their microscopic origin can be explained most consistently by atomic two-level tunneling systems carrying an electric dipole moment (*24*, *29*) and being located inside the aluminum oxide tunnel barrier of the junction (*23*). For our study, we chose a sample from the first generation of flux-biased phase qubits (*7*). These qubits were fabricated with a relatively large qubit junction of area of 32 μm^2, which means that many TLSs are present to which the qubit may couple (*23*).

We quantitatively estimated the strain fields necessary to generate noticeable changes of the TLS energy. Figure 3A shows that the corresponding frequency changes (δf_{TLS}) should be comparable or larger than the avoided level splitting; that is, on the order of 100 MHz. Going back to Eq. 2 and knowing from acoustic experiments on glasses that γ assumes values on the order of 1 eV, we find that strain fields (ε) on the order of 10^{-7} should be sufficient. On the surface of a 0.4-mm-thick substrate, such a deformation can be achieved by bending to a curvature with a radius of ~2 km; in other words, our 6.2-by-6.2–mm^2 substrate should bulge in the center by ~2.4 nm relative to the edges (*23*).

Our silicon substrate with the circuit that we studied is suspended in a notch with two opposite edges held down, whereas the center is supported and displaced by a stacked piezo element. For the force to act at a well-defined point, a small gold-plated zirconia sphere was glued on top of the piezo stack (fig. S1). Low-temperature calibration of the piezo actuator, together with numerical simulations of the chip's deformation, yields the translation factor between the strain ε in the vicinity of the qubit and the applied piezo voltage V_p to be $\varepsilon/V_p \simeq 7.8{\cdot}10^{-7}$/V (*23*). All data reported in the remainder of this paper were measured at a base temperature of 45 mK.

Qubit spectra for different piezo biases (Fig. 3C) show shifts of the avoided level crossings, whereas the qubit's resonance frequency remains unaffected. Because TLSs are expected to have a broad range of coupling strengths and no preferred orientation with respect to the strain field, different avoided level crossings change their frequencies at different rates.

To investigate the changes of TLS frequencies with applied piezo voltage more systematically, we developed the following procedure. Instead of taking whole spectra as those shown in Fig. 3A, we measured the value $P(|1\rangle)$ at the expected qubit resonance frequency f_q, known to vary as $\sqrt[4]{I_c^2 - I^2}$, for every given flux (here, I_c is the critical current of the JJ, and $I \propto \Phi_{ext}$ is the current induced in the qubit loop). Once the qubit is resonant with a TLS, the emerging avoided level crossing decreases the value of $P(|1\rangle)$ measured at f_q (Fig. 3B). A comparison with Fig. 3A shows that minima in $P(|1\rangle)$ correspond to avoided level crossings.

Figure 4A shows a series of frequency scans taken similarly to those in Fig. 3B, as a function of the piezo voltage V_p. The lighter color marks frequencies where the qubit is at resonance with a TLS. Here, the strain-tuned energy splitting of any TLS can be tracked continuously. From additional measurements in a frequency range between 11 and 13.5 GHz, we identified 41 individual TLSs. The distribution of rates at which the TLS frequencies change with piezo voltage, $\delta f_{TLS}/\delta V_p$ (Fig. 4B, inset), closely resembles a Gaussian curve centered at zero. This is expected, because, due to the random location and orientation of TLSs in the disordered AlO_x tunnel barrier of the JJ, no particular sign of the TLS frequency change is preferred when mechanical strain is applied. In terms of deformation potential γ, this distribution extends to values of $\gamma \sim \pm 0.4$ eV.

The most notable feature in Fig. 4A is a broad and curved TLS trace, whose frequency changes nonmonotonically with applied mechanical strain. The corresponding TLS resonance frequency as a function of the piezo voltage is again plotted in Fig. 4B; the data are fit to the central hypothesis of the TLS model (Eq. 2), which predicts the TLS energy splitting E to depend hyperbolically on the asymmetry energy. In our case, the asymmetry is given by $\Delta + \delta\Delta$ and defined as $\Delta + \delta\Delta = \gamma\nu(V_p - V_0)$. The fit to Eq. 2 shown in Fig. 4B yields the deformation potential of this particular TLS to be $\gamma = h{\cdot}4.72{\cdot}10^{13}$ Hz or 0.20 eV (*23*). We conclude that the applied strain moves this particular TLS through its symmetry point at which both localized atomic configurations have the same energy. Although this behavior is expected

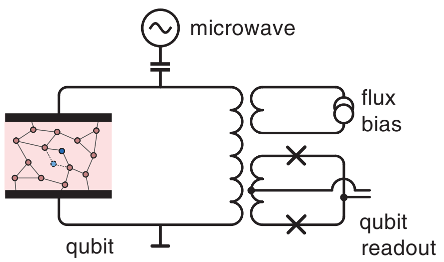

Fig. 2. Schematics of the sample circuit. The qubit consists of a superconducting loop interrupted by a JJ. The JJ is modeled as a Josephson element shunted by the intrinsic capacitor *C*. The sketch indicates the disordered structure of the JJ's tunnel barrier with an embedded TLS. The qubit is controlled by a microwave source and by the external flux, and it is read out by a dc-SQUID.

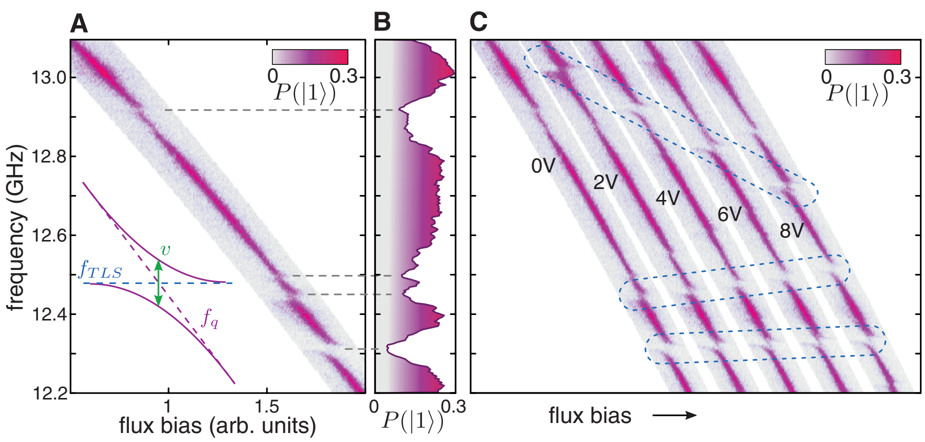

Fig. 3. Qubit spectroscopy. (**A**) Qubit spectrum as a function of the external flux Φ_{ext}. The avoided level crossings (shown schematically in the lower inset) correspond to individual TLSs coupled to the qubit. The size of the splitting v equals the coupling strength. (**B**) Probability of measuring the excited qubit state at its expected resonance frequency. Minima indicate the presence of avoided level crossings (marked by dashed lines). (**C**) Qubit spectra similar to (A), taken at five different values of the piezo voltage V_p. The spectra are shifted along the flux axis for clarity.

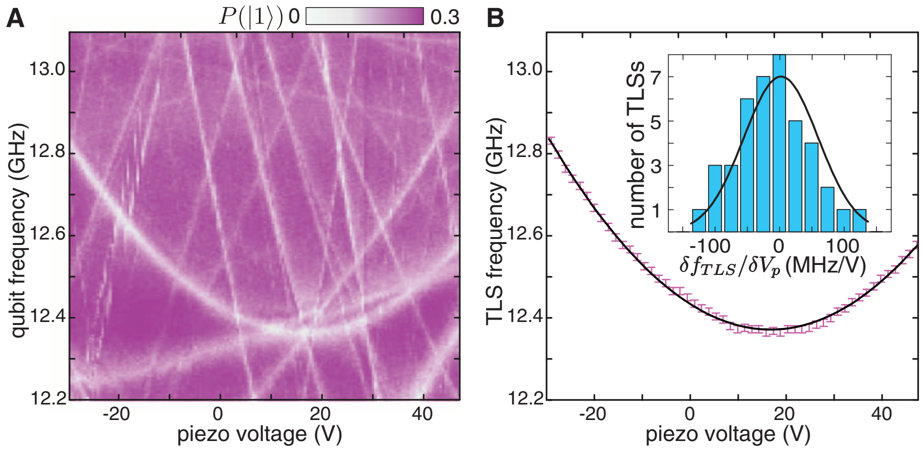

Fig. 4. Tuning two-level systems by strain. (**A**) At each value of V_p, a spectroscopic line like that shown in Fig. 3B is recorded. The resonance frequencies of the TLSs ($f_{TLS} = E/h$ as a function of V_p) appear lighter in color. The frequency dependence of the TLS showing a broad nonmonotonic behavior is extracted and fitted to a hyperbola given by Eq. 2 in (**B**). The error bars correspond to the width of the resonance dips. The inset in (B) shows the distribution of the linear frequency changes of the TLSs with respect to the voltage change; the solid line shows a Gaussian distribution for comparison.

for all TLSs, it can only be observed for TLSs that have their symmetry-point energy splitting in the accessible range limited by the tunability of the phase qubit. The other TLSs have tunnel energies Δ_0 much smaller than what is experimentally accessible; hence, only the nearly linear tails of their energy hyperbolas are observed. Data taken in the same way on another sample (fig. S4) (*23*) reveal five TLS traces obeying a hyperbolic frequency dependence on strain, showing that this is a common property of TLSs.

Another interesting trace in Fig. 4A, appearing between –30 and –10 V, indicates a TLS whose resonance frequency shifts at the rate of ~50 MHz/V and jumps randomly, within hours, between two traces ~100 MHz apart. Most likely, the local potential landscape of the coherent TLS under observation changes abruptly due to a nearby incoherent TLS fluctuating slowly and randomly between its localized states.

The basic idea of the above experiment has some similarity to earlier experiments (*30*, *31*) in which static strain was used to change the dwell times of individual incoherent TLSs (two-level fluctuators) in disordered metallic nanostructures. The experiments here are performed with individual coherent TLSs that have tunneling energies Δ_0 on the order of $k_B T$ (where k_B is the Boltzmann constant and T is temperature) and asymmetry energies Δ tunable by strain from values on the order of $k_B T$ to zero. The TLS energies E are measured directly, and their strain dependence given by Eq. 2 is confirmed.

All results presented above are explained readily by the tunneling model and, therefore, provide firm evidence of the hypothesis that atomic TLSs are the cause of avoided level crossings in the spectra of JJ qubits. Mechanical strain offers a handle to control the properties of coherent TLSs, which is crucial for gaining knowledge about their physical nature. Our method can also be used to tune TLS frequencies away from the qubit resonance and, thus, to optimize the coherence of a qubit circuit at its operation point. Moreover, the knowledge of how individual coherent TLSs are modified by strain opens an opportunity to manipulate TLSs via ultrasonic excitation.

References and Notes

1. R. C. Zeller, R. O. Pohl, *Phys. Rev. B* **4**, 2029 (1971).
2. W. A. Phillips, *J. Low Temp. Phys.* **7**, 351 (1972).
3. P. W. Anderson, B. I. Halperin, C. M. Varma, *Philos. Mag.* **25**, 1 (1972).
4. W. A. Phillips, *Rep. Prog. Phys.* **50**, 1657 (1987).
5. W. A. Phillips, Ed., *Amorphous Solids: Low-Temperature Properties* (Springer, Berlin, Heidelberg, 1981).
6. C. Enss, S. Hunklinger, *Low-Temperature Physics* (Springer, Berlin, Heidelberg, 2005).
7. R. W. Simmonds *et al.*, *Phys. Rev. Lett.* **93**, 077003 (2004).
8. J. M. Martinis *et al.*, *Phys. Rev. Lett.* **95**, 210503 (2005).
9. J. Gao *et al.*, *Appl. Phys. Lett.* **92**, 212504 (2008).
10. S. Ashhab, J. R. Johansson, F. Nori, *New J. Phys.* **8**, 103 (2006).
11. G. Zolfagharkhani, A. Gaidarzhy, S. Shim, R. L. Badzey, P. Mohanty, *Phys. Rev. B* **72**, 224101 (2005).
12. F. Hoehne *et al.*, *Phys. Rev. B* **81**, 184112 (2010).
13. O. Arcizet, R. Riviere, A. Schliesser, G. Anetsberger, T. J. Kippenberg, *Phys. Rev. A* **80**, 021803 (2009).
14. A. Lupaşcu, P. Bertet, E. F. C. Driessen, C. J. P. M. Harmans, J. E. Mooij, *Phys. Rev. B* **80**, 172506 (2009).
15. J. Lisenfeld *et al.*, *Phys. Rev. B* **81**, 100511(R) (2010).
16. T. A. Palomaki *et al.*, *Phys. Rev. B* **81**, 144503 (2010).
17. M. Neeley *et al.*, *Nat. Phys.* **4**, 523 (2008).
18. J. Lisenfeld *et al.*, *Phys. Rev. Lett.* **105**, 230504 (2010).
19. A. M. Zagoskin, S. Ashhab, J. R. Johansson, F. Nori, *Phys. Rev. Lett.* **97**, 077001 (2006).
20. G. Sun *et al.*, *Nat. Commun.* **1**, 51 (2010).
21. G. J. Grabovskij *et al.*, *New J. Phys.* **13**, 063015 (2011).
22. W. A. Phillips, Ed., in *Amorphous Solids: Low-Temperature Properties* (Springer, Berlin, Heidelberg, 1981), pp. 53–64.
23. Supplementary materials are available on *Science* Online.
24. J. M. Martinis, *Quantum Inf. Process.* **8**, 81 (2009).
25. L. Faoro, J. Bergli, B. L. Altshuler, Y. M. Galperin, *Phys. Rev. Lett.* **95**, 046805 (2005).
26. L. Faoro, L. B. Ioffe, *Phys. Rev. B* **75**, 132505 (2007).
27. R. de Sousa, K. B. Whaley, T. Hecht, J. von Delft, F. K. Wilhelm, *Phys. Rev. B* **80**, 094515 (2009).
28. J. H. Cole *et al.*, *Appl. Phys. Lett.* **97**, 252501 (2010).
29. J. S. Kline, H. Wang, S. Oh, J. M. Martinis, D. P. Pappas, *Supercond. Sci. Tech.* **22**, 015004 (2009).
30. N. O. Birge, J. S. Moon, D. Hoadley, *Czech. J. Phys.* **46**, 2343 (1996).
31. S. Brouër, G. Weiss, H. B. Weber, *Europhys. Lett.* **54**, 654 (2001).

Acknowledgments: We thank M. Ansmann and J. M. Martinis (University of California, Santa Barbara) for providing the sample we measured in this work and J. H. Cole, E. Demler, Y. M. Galperin, M. D. Lukin, J. M. Martinis, R. McDermott, J. E. Mooij, C. Müller, A. Shnirman, and J. Wrachtrup for fruitful discussions. This work was supported by the DFG and the State of Baden-Württemberg through the DFG CFN, as well as by the European Union project SOLID.

Supplementary Materials

www.sciencemag.org/cgi/content/full/338/6104/232/DC1
Supplementary Text
Figs. S1 to S4
References (*32*–*35*)

25 June 2012; accepted 6 September 2012
10.1126/science.1226487

Observation of Resonances in Penning Ionization Reactions at Sub-Kelvin Temperatures in Merged Beams

A. B. Henson, S. Gersten, Y. Shagam, J. Narevicius, E. Narevicius*

Experiments have lagged theory in exploring chemical interactions at temperatures so low that translational degrees of freedom can no longer be treated classically. The difficulty has been to realize in the laboratory low-enough collisional velocities between neutral reactants to access this regime. We report here the realization of merged neutral supersonic beams and the manifestation of clear nonclassical effects in the resulting reactions. We observed orbiting resonances in the Penning ionization reaction of argon and molecular hydrogen with metastable helium, leading to a sharp absolute ionization rate increase in the energy range corresponding to a few degrees kelvin down to 10 millikelvin. Our method should be widely applicable to many canonical chemical reactions.

Theoretical quantum chemistry suggests that at low-enough collision energies, where reactants' de Broglie wavelength approaches the characteristic interaction length scale, quantum effects, such as tunneling through reaction or centrifugal barriers, will dominate the reaction